Some metallurgical aspects of Dynamic Strain Aging effect on the Low Cycle Fatigue behavior of C–Mn steels

Zhiyong Huang, Danièle Wagner, Claude Bathias

HAL Id: hal-01687050
https://hal.parisnanterre.fr/hal-01687050v1

Submitted on 18 Jan 2018

Some metallurgical aspects of Dynamic Strain Aging effect on the Low Cycle Fatigue behavior of C–Mn steels

Z. Huang [a,b], D. Wagner [a,*], C. Bathias [a]

[a] *University Paris Ouest Nanterre, LEME Laboratory, 50, rue de Sèvres, 92410 VILLE D'AVRAY, France*
[b] *Sichuan University, School of Aeronautics and Astronautics, No. 29 Jiuyanqiao Wangjiang Road, Chengdu 610064, China*

ABSTRACT

Carbon–Manganese steels and associated welds are commonly used, and sometimes to sustain loads in the Low Cycle Fatigue domain. Nevertheless, the metallurgy of these C–Mn steels is rather complex, due to the interaction of solute atoms (carbon and nitrogen) with dislocations during deformation which leads to metallurgical instabilities: Lüders strain, Static Strain Aging (SSA) and Dynamic Strain Aging (DSA). The DSA phenomenon is an interaction during the test between solute atoms and dislocations which are submitted to an supplementary anchorage if the temperature is sufficient to allow the diffusion of solute atoms leading to a discontinuous plastic deformation localized in bands associated with serrations on the stress–strain curve. In C–Mn, the temperature domain where the phenomenon is present is from 150 °C to 300 °C. If these metallurgical instabilities induce an increase in hardness, unfortunately they produce a decrease of ductility detrimental to components safety. The results of the DSA effect on LCF behavior in C–Mn and Low Alloyed steels reported in the literature are very confused and contradictories. In this study, two C–Mn steels with a different sensitivity to DSA are investigated in the Low Cycle fatigue domain. As reported from some authors, the fatigue life seems enhance or reduce in the temperature domain where the DSA is maximum, but the decrease of the strain rate always decreases the number of cycles to failure.

Keywords:
Carbon manganese steels
Dynamic Strain Aging
Low Cycle Fatigue
Solute atoms

1. Introduction

Carbon–manganese steels, in the form of pipes, plates and forgings, and associated welds are commonly used for heat exchangers in pressurized water reactors secondary systems (feedwater line and steam line). These lines are currently submitted to cyclic amplitude loadings inferior to the yield stress and fatigue limit, but may also occasionally sustains high amplitude loadings in the Low Cycle Fatigue domain during transient operating conditions.

Nevertheless, the metallurgy of these C–Mn steels is rather complex, due to the interaction of solute atoms with dislocations during deformation which leads to metallurgical instabilities: Lüders strain, Static Strain Aging (SSA) and Dynamic Strain Aging (DSA). If these metallurgical instabilities induce an increase in hardness, unfortunately they produce a decrease of ductility detrimental to components safety [1–10].

The Lüders strain appears at the transition between elastic and plastic domain in the 20–200 °C temperature range. At the upper Yield Stress, the stress drops suddenly and in the sample the plastic deformation begins at one side of the specimen and propagates as a plastic front all the length sample. If during the homogeneous plastic deformation, an unloading is done followed by a heat treatment around 200 °C during few minutes, and a reloading is performed, the Static Strain Aging (SSA) takes place. It results in the return of the Lüders strain phenomenon. These phenomena (Lüders and SSA) being observable at room temperature, they are well observed. After that, the plastic deformation is homogeneous during the test until the reduction of area beginning.

In the Dynamic Strain Aging (DSA) phenomenon, the aging is sufficiently rapid to occur during straining. In this case, for the most sensitive materials to the DSA, the localization of the strain is characterized in a tensile test by the formation and the propagation of plastic strain bands called Portevin-Le Chatelier bands (PLC bands). During a tensile test at imposed strain rate, DSA phenomenon is associated with serrations on the stress–strain curve [11–17]. Each stress drop on the tensile curve corresponds to the formation of a band. These serrations on the stress–strain curve can be classified in three types depending on the spatiotemporal appearance of these bands [12–15]. The type C corresponds to the chaotic formation of the bands (discontinuous and not

correlated). Each stress drop on the tensile curve corresponds to the formation of one band. The type B corresponds to the discontinuous but regular formation of the bands (each new band is created just near the previous band and so on). Each created band is characterized by a stress drop on the stress–strain curve too. Type A band corresponds to a continuous propagation of a band along the specimen. With each type of band (A, B or C) is associated a type of serration on the stress–strain curve, more or less easily identifiable. The occurrence of these different types of bands which correspond to various spatiotemporal types of localization depends on external parameters (level of strain, strain rate, temperature, stiffness of the tensile machine, geometry and surface quality of the samples) and internal parameters (alloy composition, crystal lattice, standard structure, solute atoms type and content, density of mobile dislocations, types of obstacles, grain size). At a microscopic strain, this DSA phenomenon is explained by the interaction of mobile dislocations with the interstitial solute atoms. The dislocation gliding is not continuous, but discontinuous [18–22]. Dislocations are temporarily stopped on the obstacles (forest, precipitates...) for a waiting time t_w, during which the diffusion of the solute atoms creates an additional anchoring of dislocations. So, the phenomenon is active in a domain of strain rate (which impose the dislocations speed) and temperature (which impose the diffusion of solute atoms). In C–Mn steels [22], the DSA phenomenon occurs for common strain rate (10^{-4}–10^{-1} s^{-1}) in a temperature range of 150–300 °C which makes the observation difficult [9,10]. To measure the sensitivity to DSA, tensile tests and more accurate strain rate sensitivity tests are needed [23] in the temperature domain where DSA occurs. Indeed, inside the DSA domain (in temperature and strain rate), there exists a more restricted domain where the strain rate sensitivity coefficient $S = \frac{\Delta \sigma}{\Delta Log \dot{\varepsilon}}$ is negative. It is when S becomes negative that the Portevin-Le Chatelier bands occur [22].

In C–Mn steels, it is well established that the atoms which interact with dislocations are carbon and nitrogen. Due to its greater solubility limit, nitrogen seems to exert a more pronounced influence on strain aging than carbon does [1,5,24,25].

So, the strain localization induced by Lüders, SSA and DSA phenomena is correlated to external parameters: strain, strain rate, temperature, stiffness machine, geometry samples, surface roughness, and internal parameters: chemical composition, crystal lattice, type and content of solute, mobile dislocation density, obstacles type (forest, precipitates...), grain size, single or polycrystal. The primordial parameters are strain rate, temperature, chemical composition (C, N, Al, Mn content, see Section 2), type (diffusion coefficient) and content of solute atoms.

The results of the DSA effect on LCF behavior in C–Mn and Low Alloyed steels reported in the literature are very confused and contradictory [26–30].

In the Low Cycle Fatigue (LCF) tests, the first indication of DSA for the most sensitive alloys is serrated yielding on the hysteresis loop (stress amplitude versus strain amplitude). Abdel Raouf [26] on a Ferrovac E iron with 0.007% C, 3 ppm N and 0.01% Al which DSA maximum peak in tensile tests occurs at 370 °C reports that the stress–strain loops were very heavily serrated. Samuel et al. [30] show the hysteresis loop obtained with a SA 333 gr 6 steel where the nitrogen and carbon content are respectively 0.01% and 0.14%. Neither the aluminium content is given, nor the temperature of maximum UTS. Theses authors reported that serrated flow is observed at all temperatures (between 30 and 400 °C) except at room temperature. In this case, the number of cycles to failure N_f increases between 20 and 275 °C and decreases for higher temperature. This trend is equally reported by Abdel Raouf [26]. The evolution of the stress amplitude or maximum stress is also an interesting parameter. In DSA domain, generally a first hardening is observed at the beginning of the test followed by stabilization and a possible second hardening. This second hardening is attributed to DSA. A strong effect of the strain rate is reported. Depending of the temperature, with decreasing the strain rate, the fatigue life may be either unaffected, either decreased, or increased.

For most references, neither the hysteresis loop neither the evolution of the Ultimate Tensile Stress (UTS) with temperature and strain rate coefficient are given. Moreover, some important parameters owing to characterize the DSA effect are missing (chemical composition...) and it is impossible to have clear ideas on the DSA effect on the Low Cycle Fatigue behavior for C–Mn steels (and Low Alloyed steels). So, in this article, we have performed Low Cycle Fatigue tests on two C–Mn steels well characterized previously and whose DSA sensitivity is different.

2. Materials

The materials studied are two carbon–manganese steels of AFNOR (French standard) NFA 36205 grade A48 and A42 which were received as 40 mm thick plates. The chemical composition is reported in Table 1. The plates received a prior normalization thermal treatment consisting in austenitizing at 870 °C then air cooling, leading to a microstructure composed of banded ferrite and pearlite.

The A48 grade material is a silicon semi-killed steel containing a very low aluminium content (0.004%). This element is in insufficient amount to be capable of trapping nitrogen atoms by aluminium nitride (AlN) formation during cooling from the austenitic domain. Consequently, for this heat a large amount of free nitrogen is still present in the lattice making this alloy sensitive to DSA. The A42 grade material is a fully-killed steel containing aluminium content (0.045%) and for this amount of aluminium, almost the whole of nitrogen atoms are trapped as aluminium nitrides making this alloy much less sensitive to DSA.

In C–Mn steels, it is well established that the atoms which interact with dislocations are carbon and nitrogen. According to its greater solubility limit, nitrogen seems to exert a more pronounced influence on aging than carbon does [1,5,24,25]. The localization of these atoms is rather complex [9,10]. One part is precipitated in the form of carbides (Fe$_3$C...) or nitrides (Fe$_4$N, Fe$_{16}$N$_2$ or AlN if aluminium is present). The other part is in solid solution into the centered cubic iron lattice. This part in solid solution is distributed into 3 locations [31–34]: the majority of the atoms gathers and form the "Cottrell atmospheres", a few part segregates on dislocations in the interstitial sites, and the remained solute atoms (when all sites near dislocations are occupied) are free in the lattice interstitial sites. It seems that solute atoms in "Cottrell atmospheres" are responsible for the Lüders strain and Static Strain Aging. On the other hand, it has been demonstrated that in C–Mn steels, it is the free carbon and nitrogen in the interstitial sites which are responsible for Dynamic Strain Aging phenomenon [23] in the majority of the cases.

3. Experimental procedure

3.1. Tensile tests

Tensile tests were carried out in the 20–300 °C (for the A48 steel) or 350 °C (for the A42 steel) temperature range with a strain rate of 2.4 10^{-4} s^{-1}.

3.2. Strain rate sensitivity tests

The used method for the determination of the Strain Rate Sensitivity coefficient $S = \frac{\Delta \sigma}{\Delta Log \dot{\varepsilon}}$ was the strain rate $\dot{\varepsilon}$ drop at a

Matériau	C	S	P	Si	Mn	Ni	Cr	Mo	Cu	Sn	Al	N	O
A42	0.140	0.0057	0.016	0.225	0.989	0.024	0.021	0.002	0.027	0.003	0.045	0.0082	0.0006
A48	0.198	0.012	0.0104	0.207	0.769	0.135	0.095	0.025	0.273	0.023	0.004	0.0083	0.0049

constant temperature and a given deformation. In this study, the drop in $\dot{\varepsilon}$ (from $\dot{\varepsilon}_1 = 2.4 \cdot 10^{-4}$ s^{-1} to $\dot{\varepsilon}_2 = 2.4 \cdot 10^{-3}$ s^{-1}) was always carried out at a deformation of 4%. Tests were conducted at various temperatures from 20 °C to 300 °C or 350 °C.

3.3. Internal friction tests

The internal friction technique allows to study the mobility of the defects present in the crystalline structure under loading well below the Yield Stress. It is among possible to evaluate the balance between free carbon and nitrogen atoms in the lattice and carbon and nitrogen atoms interacting with mobile dislocations. Internal friction experiments were performed in the −20 to 300 °C temperature range on an inverted torsion pendulum [37] with an applied strain of $5 \cdot 10^{-6}$ and a heating rate of 130 °C per hour on circular samples (3 mm diameter, 50 mm gage length) whose geometry leads to a resonant frequency of the apparatus close to 1.5 Hz. The internal friction parameter Q^{-1} which is related to the dissipated energy lost by the defects mobility, is recorded as a function of the test temperature.

### 3.4. Low Cycle Fatigue tests

Total strain-controlled fatigue tests were carried out in air in a closed loop servo hydraulic fatigue test machine (Instron 8500). Low cycle fatigue specimens were designed as Fig. 1 shows. In the middle of the specimen, the extensometer is located on a 12 mm length. The specimen is controlled by strain with triangular wave form ($R = -1$). The applied total strain range was varied from 0.3% to 1%, the temperature of tests from 20 °C to 200 °C, and the strain rate from 3.2×10^{-4} (0.01 Hz) to 3.2×10^{-2} s^{-1} (1 Hz). The specimens were heated in a classical furnace. The number of cycles to failure N_f was measured when the stress amplitude dropped 20% after cyclic saturation under strain controlled loading.

All data are saved to computer by the data acquisition system and its storage format is Excel.

4. Results

4.1. Tensile tests

On the conventional tensile curves (nominal stress versus strain $\Delta L/L_o$, the Portevin-Le Chatelier effect (PLC) is clearly exhibited at both 100 and 200 °C for the A48 steel whereas for the A42 steel no serrations resulting from the PLC effect were visible. The variations of the ultimate tensile strength σ_{UTS} and the total elongation are plotted versus temperature in Figs. 2 and 3 for the two steels. In
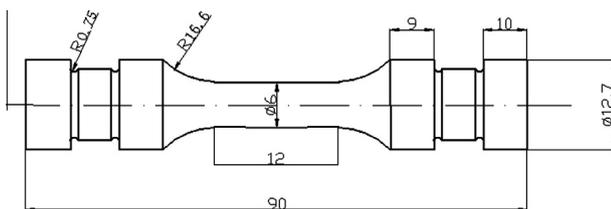
Fig. 1. Design specimen for the test.
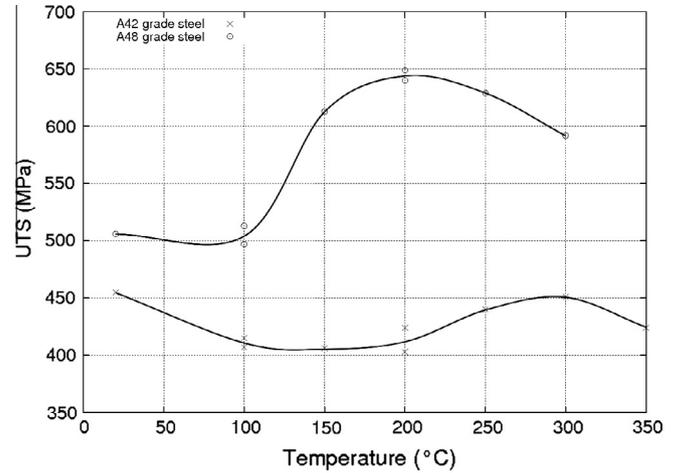
Fig. 2. Ultimate tensile strength versus temperature for semi-killed A48 steel and fully-killed A42 steel.
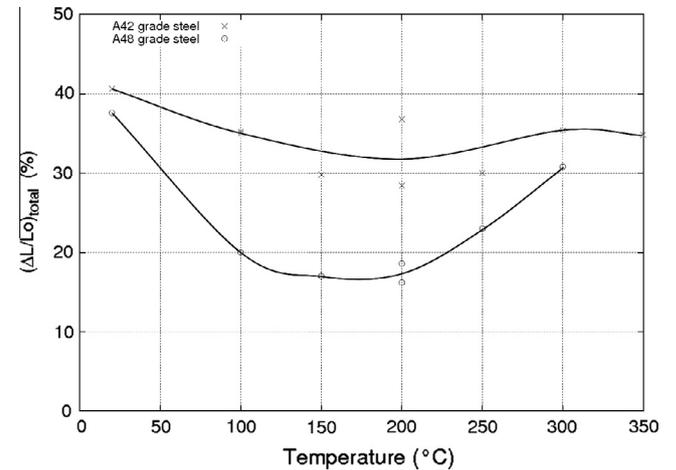
Fig. 3. Total elongation versus temperature for semi-killed A48 steel and fully-killed A42 steel.

the temperature range tested, the two steels display UTS maxima associated with elongation minima, but the maximum and the minimum are more pronounced in the A48 steel than in the A42 steel. According to the more important manganese content [9] of the A42 steel, the UTS maximum and the elongation minimum are shifted to higher temperature (250–300 °C for the UTS of the A42) compared to 200 °C for the A48, and 200 °C for the elongation of the A42 compared to 150 °C for the A48. Indeed, interactions between manganese atoms and nitrogen (and carbon) atoms seem to exist. They reduce the mobility of the nitrogen and carbon atoms which induces higher temperature.

4.2. Strain rate sensitivity tests

Fig. 4 gives the evolution of the strain rate sensitivity S versus temperature for the two steels. According to the tensile tests, for the silicon semi-killed A48 steel, S shows a sharp minimum in
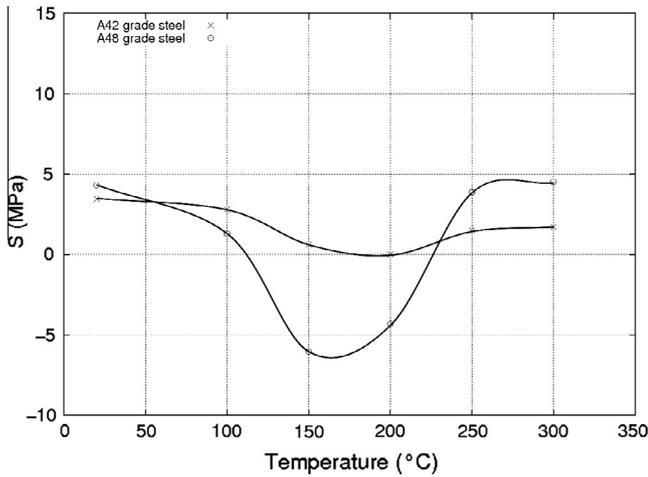
Fig. 4. Strain rate sensitivity coefficient versus temperature for semi-killed A48 steel and fully-killed A42 steel.

the temperature range tested whereas for the aluminium killed A42 steel, this minimum is less pronounced. As expected, the minimum of S occurs at the same temperature that the one observed elongation (200 °C for the A42 and 150 °C for the A48).

4.3. Internal friction tests

The internal friction spectrum measured on the A48 grade reveals two main peaks in the −20 to 300 °C temperature range (Fig. 5, curve 1). The first one which presents a maximum at about 20 °C can be associated with the Snoek Peak (SP) resulting from carbon and nitrogen redistribution between octahedral sites in
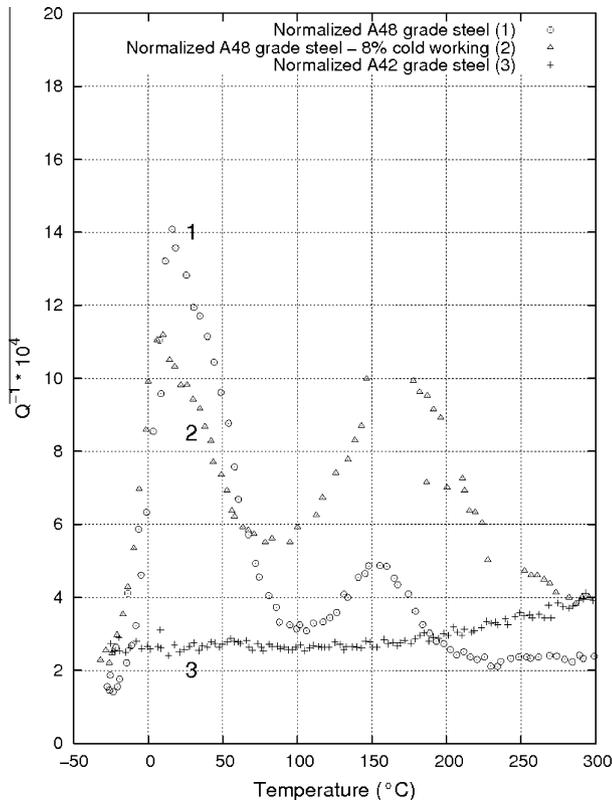

Fig. 5. Internal friction Q^{-1} versus temperature for A48 (normalized and cold worked conditions) and A42 steels.

the ferritic lattice [35]. Due to complex interactions between nitrogen and manganese, the Snoek Peak height is not directly proportional to C and N interstitial content in the lattice, as observed in pure iron. The second peak, observed in the 150–250 °C temperature range, corresponds to the Cold Work Peak (CWP) and is due to the interaction between dislocations and interstitials such as carbon and nitrogen [35]. The CWP height is related to both the density of mobile dislocations and the interstitial content in the vicinity of dislocations. This classical interpretation of the internal friction spectrum in steels is confirmed by curve 2 which represents the internal friction variation measured on this A48 grade steel after 8% cold working and one month room temperature aging. In that case, an increase of the CWP with dislocation density is observed, associated with a corresponding SP decrease, in agreement with the classical balance of interstitial atoms between lattice and dislocations [35].

The internal friction spectrum measured on the A42 grade (curve 3) reveals no peak (neither SP nor CWP) in agreement with the nitrogen content in the ferritic lattice.

4.4. Low Cycle Fatigue tests

4.4.1. Influence of the temperature

At room temperature, the hysteresis loop (stress amplitude–strain amplitude) does not show serrations (Fig. 6), whereas from 100 °C (Fig. 7), whatever the material (A42 or A48), it appears serrations in the plastic domain. For a strain rate of 4×10^{-3} s^{-1}, these serrations are regular and occur from the first cycle.

As previously reported in the literature [28], the evolution of the maximum stress with the number of cycles presents a first hardening followed by a stabilization or a second hardening (Figs. 8 and 9). At room temperature and 100 °C, the second hardening is weak. From 150 °C, the second hardening increases and at 200 °C, for the A48 steel, a softening regime appears between the two hardenings.

The evolution of the maximum stress amplitude obtained during the test ($\Delta\sigma_{max} = \sigma_{max} - \sigma_{cycle\ 1}$) is plotted with the temperature on the Fig. 10 for a strain amplitude of 0.8% and a strain rate of 3.2×10^{-3} s^{-1} or 4×10^{-3} s^{-1}. For the two steels, the maximum stress amplitude due to hardening increases when the temperature increases between 100 °C and 200 °C. For A48 steel where a test at 100 °C has been performed, this maximum decreases slightly between 20 °C and 100 °C. This maximum stress amplitude is higher for the most sensitive steel to DSA (A48) in good agreement with the higher increase in UTS measured on a tensile test in temperature.
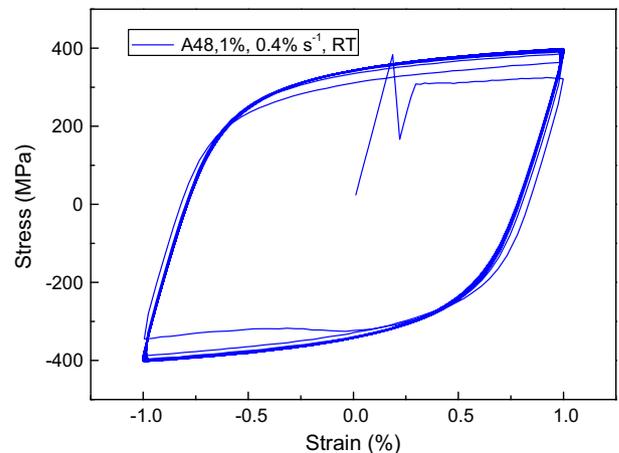

Fig. 6. Hysteresis loop for A48 steel at room temperature (1% strain amplitude, 0.4% s^{-1} strain rate).
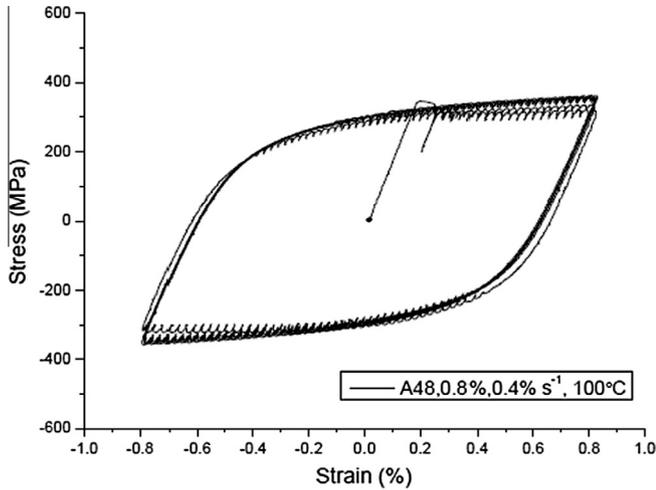
Fig. 7. Hysteresis loop for A48 steel at 100 °C (0.8% strain amplitude, 0.4% s^{-1} strain rate).

Fig. 11 shows the correlation between the maximum stress amplitude measured in the LCF tests at each temperature (for $\Delta\varepsilon_t/2 = 0.8\%$) and the increase in UTS at each temperature (UTS^{T} – UTS$^{20°C}$).

If we see the evolution of the number of cycles at fracture N_f with the temperature (with a strain rate in the domain of 10^{-3} s^{-1}), we notice that N_f increases with the temperature (Fig. 12) for the two steels, and the increase is most important for the most sensitive steel. For the A48 steel, it seems to occur a minimum of N_f at the temperature of 150 °C with a same tendency for the A42 steel. This minimum occurs at the minimum of ductility in tensile testing.

4.4.2. Influence of the strain

For the A48 steel, the $\Delta\sigma_{max}$ was plotted at room temperature with the strain amplitude on the Fig. 13. Higher the strain amplitude, higher the maximum stress amplitude. For the A42 steel, the increase of the $\Delta\sigma_{max}$ is less important.

4.4.3. Influence of the strain rate

The evolution of the maximum stress amplitude obtained during the test is plotted with the strain rate on the Fig. 14. Even at room temperature (for the two materials), the maximum
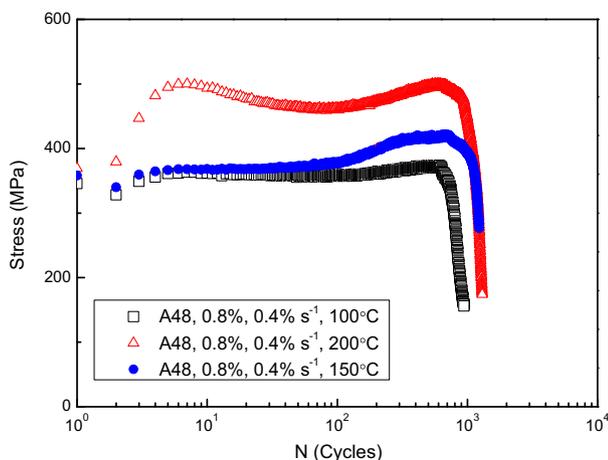
hardening decreases when the strain rate increases leading to a negative Strain Rate Sensitivity. At 200 °C for the A48 steel, the decreasing of the maximum hardening between 4×10^{-4} and 4×10^{-3} s^{-1} is drastic. On the Fig. 15, the hysteresis loop (stress amplitude–strain amplitude) at 200 °C and for the lowest strain rate shows different serrations compared to the serrations for higher strain rate (Fig. 7). These serrations seems to be serrations corresponding to bands of type C.

If we look at the evolution of the number of cycles at fracture N_f with the strain rate (Fig. 16), we notice that N_f increases when the strain rate increases at RT and in a more important manner at 200 °C. The conventional presentation of the LCF results (Manson Coffin curve) (Fig. 17) shows equally the important effect of the strain rate for the A48 steel at 200 °C.

5. Discussion

5.1. Temperature effect

Taking into account the strain amplitude in the Low Cycle Fatigue tests (strain amplitude in the Lüders strain), all aging types (Lüders, Static Strain Aging and Dynamic Strain aging) are involved in the Low Cycle Fatigue behavior.

From Lee [28], the first hardening is caused by cyclic strain hardening and the second hardening is due to dynamic strain aging. Mughrabi [36] reporting some literature results and more particularly those of Weisse [27] explains the DSA effect on the dislocation distribution during the fatigue tests on plain carbon and α-iron. The dislocation distribution observed by transmission electron microscopy in specimens tested in stress or strain amplitude control at 25, 275 and 375 °C shows that below or above the DSA domain, a cell/subgrain structure is observed, whereas at temperature of maximum DSA, a dense wall/vein structure is observed. In the case of tests at constant plastic strain amplitude, instead of the formation of a dominant wall/vein structure in the DSA regime, a "labyrinth type" wall structure is observed. In the DSA domain [36], because of thermal activation increase, the mobility of the screw dislocations would be higher. At the same time, the edge dislocations would become less mobile because of the interaction with the solute atoms (for which diffusion is sufficiently high). Thus, the mobility of edge and screw dislocations would be comparable. The overall dislocation density would be expected to be much larger than in the case of a dislocation cell structure. The most significant consequence of the DSA is to produce a higher dislocation density which induces the secondary hardening. The
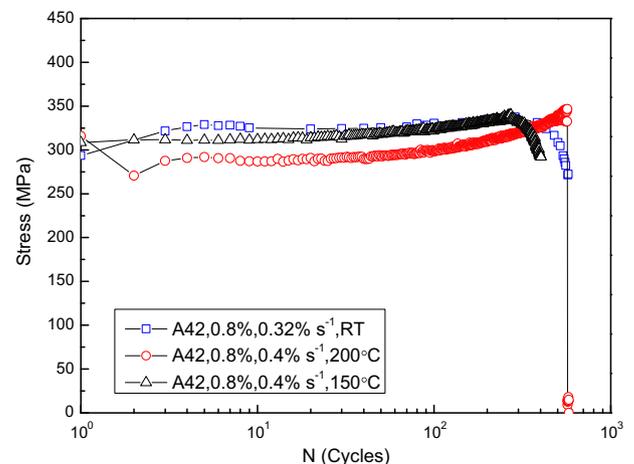

Fig. 8. Stress evolution during the test for the A48 steel at 100 °C, 150 °C, 200 °C (0.4% s^{-1} strain rate).
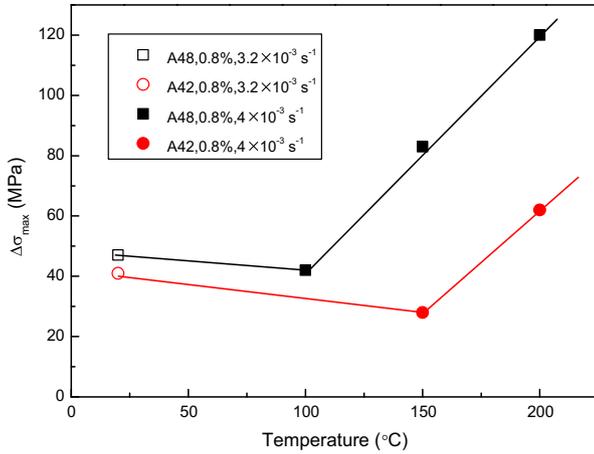

Fig. 9. Stress evolution during the test for the A42 steel at RT, 150 °C, 200 °C (0.4% s^{-1} strain rate).

Fig. 10. Maximum stress amplitude evolution for A48 and A42 steels with the temperature.

Fig. 12. Evolution of the number of cycles at fracture with the temperature for the 2 steels.

veins/walls are assumed to be the obstacles for arresting dislocations during a waiting time t_w, and during this waiting time, the diffusion of the solute atoms creates an additional anchoring of the dislocations. Higher is the solute atoms, higher is the secondary hardening as the Fig. 10 shows for the steels tested in this study.

5.2. Strain rate effect

The strain rate effect on the maximum amplitude stress (Fig. 14) shows clearly a negative strain rate sensitivity for the two steels even at room temperature (weakly) and very important at 200 °C in agreement with the S results (Fig. 3). The LCF behavior is identical to the monotonic tensile behavior. When the strain rate decreases, the value of the UTS increases as well as the temperature where the UTS is maximum [3]. The DSA phenomenon is active in a domain of strain rate (which imposes the dislocation speed) and temperature (which imposes the diffusion of solute atoms). In the DSA domain, when the strain rate decreases, the content of anchored solutes atoms increases and the waiting time of the dislocations increases, and higher are the UTS and the secondary hardening. The discontinuous glide of dislocations can be seen by the serrations on the curve. When the strain rate decreases (the waiting time of dislocations increases) or the temperature increases (mobility of diffusing species increases) the localization of the bands evolves from the type A to the type B, then type C.
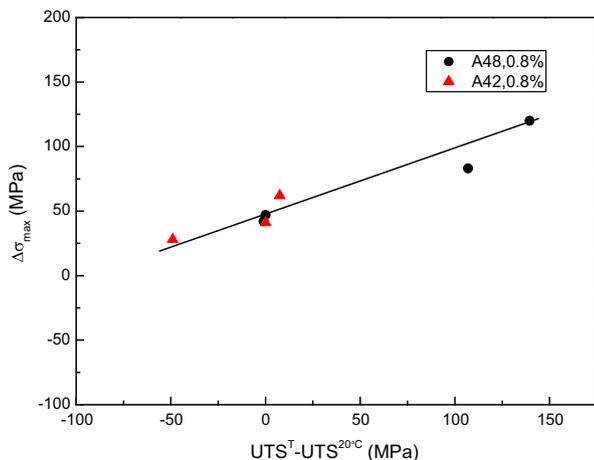
Today, the transition between these various types of bands are not still clearly explained. The type A serration corresponds to a weak anchorage of the dislocations (low temperature, high strain rate) whereas the type C corresponds to a strong anchorage of solute atoms by the dislocations. In this study, the serrations type on the hysteresis loop are of type B for a strain rate of 3.2×10^{-3} s^{-1}; except for one test (A 48 steel at 200 °C and a strain rate of 4×10^{-4} s^{-1}) where the serrations seem to be type C (chaotic formation of the bands) that is to say serrations corresponding to a strong anchorage. In this later case, the second hardening due to DSA (seen by the maximum stress amplitude) is important as shown by Fig. 14. These results are in good agreement with the literature review [26,27,30].

5.3. Dynamic Strain Aging effect on the fatigue life

In this study, at a strain rate of 4×10^{-3} s^{-1}, the fatigue life N_f (Fig. 12) increases from RT to 100 °C, decreases at 150 °C and increases at 200 °C. The fatigue life seems higher in the DSA domain. This fatigue life is strongly reduced by the decrease of the strain rate (Fig. 16), but even at a strain rate of 3.2×10^{-4} s^{-1}, the fatigue life is of the same order or higher at 200 °C than at RT. This same trend has been observed by Lee and Kim [28] on a SA 508 Cl3 with 0.18% C (the N, Al and Mn contents are not given). From their results, this steel is less sensitive to DSA

Fig. 11. Correlation between the maximum stress amplitude (LCF tests) and the increase of UTS (tensile tests) for different temperatures.
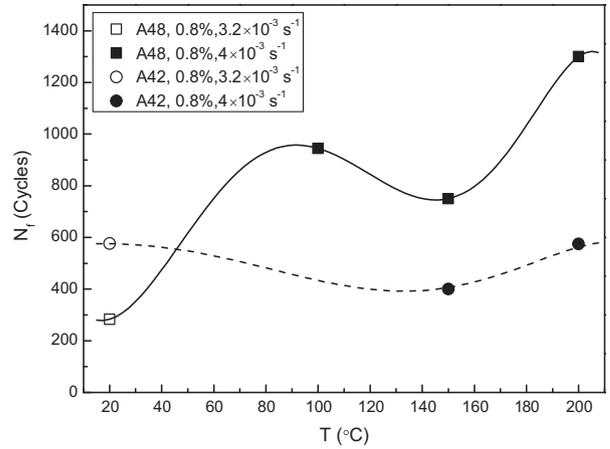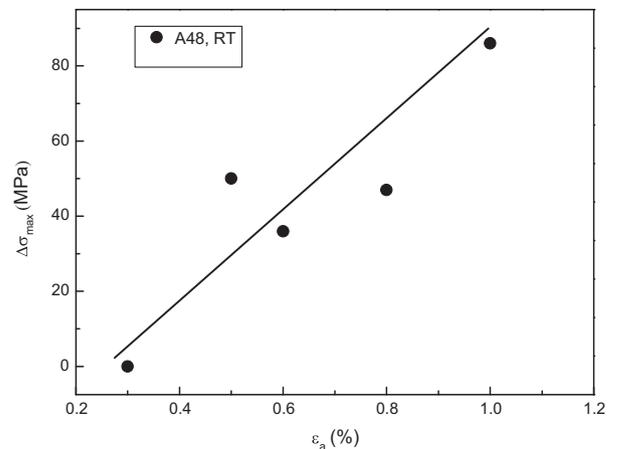

Fig. 13. Evolution of the maximum stress amplitude with the strain amplitude for the A48 steel at room temperature.

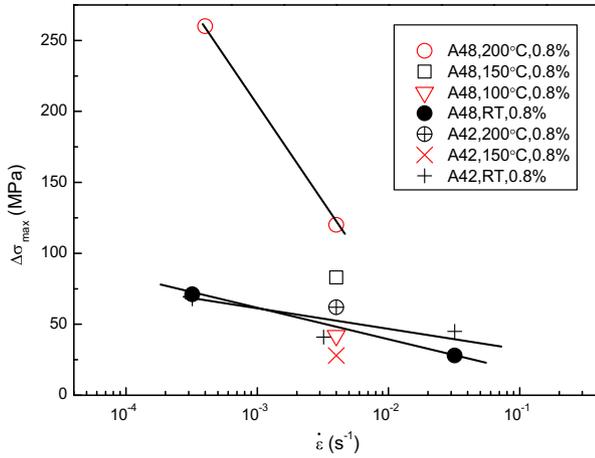**Fig. 14.** Maximum stress amplitude evolution with the strain rate for the 2 steels at different temperatures.

Fig. 16. Number of cycles at fracture N_f evolution with the strain rate (0.8% stain amplitude) for the 2 steels at different temperatures.

than our C–Mn steels (only at 300 °C a secondary hardening appears). In this case, the fatigue life (for $\Delta\varepsilon_t/2 = 2\%$) at 300 °C (probable temperature of maximum DSA in tensile) is of the same order than the fatigue life at RT, and show a minimum at 150 °C. On the other hand, Abdel-Raouf et al. [26], Weisse et al. [27] and Samuel et al. [30] find a fatigue life which increases and then decreases with temperature, but the increase is at a $T < T_{DSA}$, and the decrease corresponds to the T_{DSA}. The overall results are compared on the Fig. 18 with our results for different strain rates. Abdel Raouf et al. [26] have performed tests on a Ferrovac iron with 0.007% C, 3ppm N, 0.01% Al and 0.001% Mn. The evolution of the UTS with temperature is not given. These authors reported that a secondary hardening occurs even at 20 °C which is surprising. The evolution of the steady state stress amplitude between the first and the second hardening shows a maximum stress at a temperature of 375 °C which is abnormally high for this steel with very few C, N and Mn content. The results are given (Fig. 18) for a plastic strain amplitude of 2% for a strain rate of 4×10^{-4} and $1.6 \times 10^{-3} \text{ s}^{-1}$. Weisse et al. [27] have performed their tests on a SAE 1045 steel which exact composition is not given. The maximum UTS in tensile is located at 265 °C. With the evolution of their UTS with temperature, it seems that this steel is not very sensitive to DSA phenomenon [23] ($\text{UTS}^{max} - \text{UTS}^{min} \approx 80 \text{ MPa}$) compared to
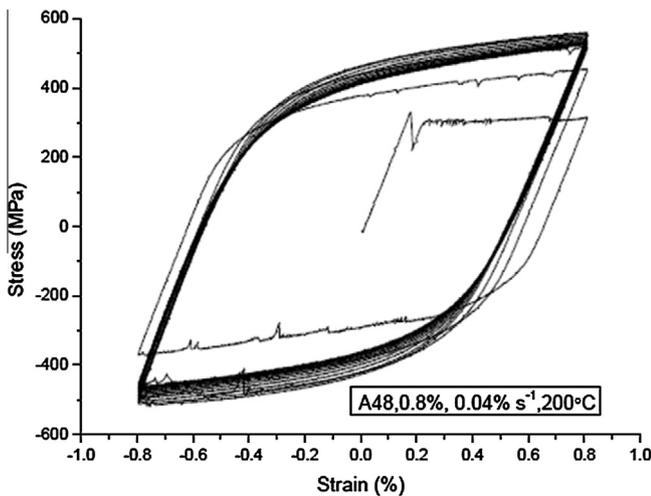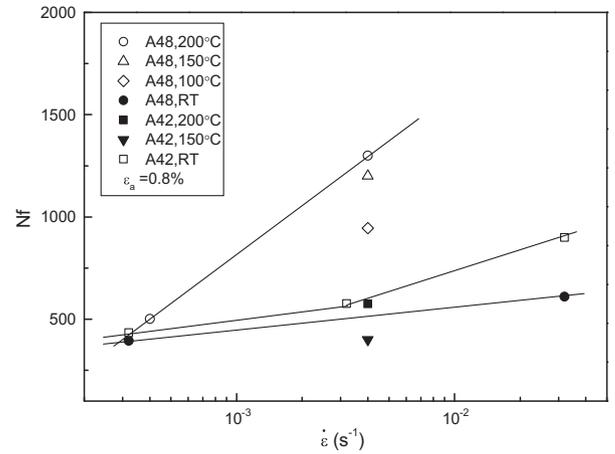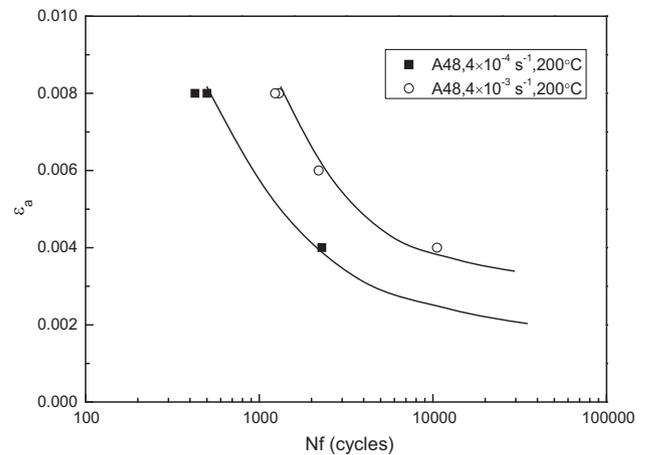

Fig. 17. Effect of the strain rate on the Manson Coffin curve (strain amplitude – number of cycles at failure N_f for the A48 steel).
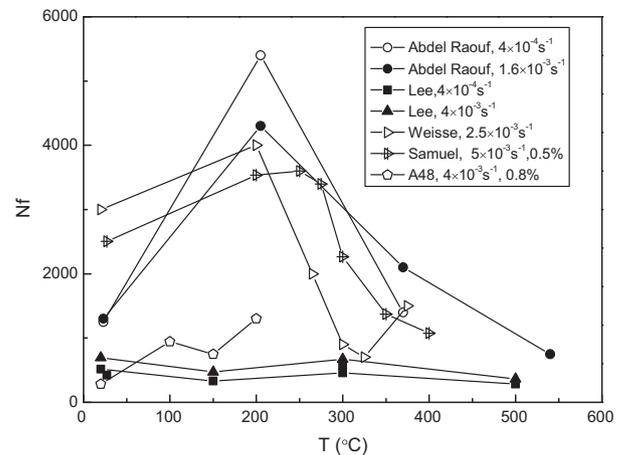

Fig. 18. Evolution of the number of cycles at failure with the temperature (from different authors) and comparison with our results on the A48 steel.

Fig. 15. Hysteresis loop for A48 steel at 200 °C (0.8% strain amplitude, 0.04% s^{-1} strain rate).

our A48 steel ($\text{UTS}^{max} - \text{UTS}^{min} \approx 150 \text{ MPa}$). The shown results (Fig. 18) are for a plastic strain amplitude of 0.5% for a strain rate of $0.5 \times 10^{-2} \text{ s}^{-1}$. Samuel et al. [30] have performed tests on a SA 333 gr 6 with 0.14% C, 0.01% N, 0.9% Mn (Al content is not

reported). The evolution of the UTS and ductility with temperature are not given. The evolution of the stress amplitude with the number of cycles shows a maximum at 350 °C at a strain rate of $5 \times 10^{-3}\,s^{-1}$ and a total strain amplitude of 0.5%. For all these references, the sensitivity of the studied steels regarding the DSA phenomenon is not quantified, and the tests were performed at different strains amplitudes and strain rates. The evolution of the UTS and total strain in tensile with the temperature are not given.

From Hertzberg et al. [38], for a total strain amplitude above 1%, the ductility is the more influent parameter to improve the fatigue life in the LCF domain, whereas at strain amplitudes below 1%, it will be the hardness which improve the fatigue life. The tests presented here are for a total strain amplitude of 0.8% and a competition between ductility and hardness occurs. For the less sensitive steel A42, the fatigue life is unchanged between 20 and 200 °C, the ductility loss and the hardness increase makes up each other. For the more sensitive steel A48, the fatigue life is minimum at the ductility minimum (150 °C, Fig. 12), but it increases at 200 °C by the hardness increase.

For Lee and Kim [28], the fracture path appearance is different at RT, 300 °C and 500 °C.]The striation width at 300 °C is nearly equal to that at RT, and much narrower than that at 500 °C. These authors concluded that the crack propagation rate at 300 °C is equal to that at RT. It increases at 200 °C by the hardness increase higher than at 500 °C. In the DSA domain, the overall fatigue resistance was increased by crack branching (although DSA promoted the crack initiation) and a slower crack propagation rate.

6. Conclusions

Two C–Mn steels with different sensitivity to DSA phenomenon were studied in the low cycle fatigue domain between 20 and 200 °C with different strain rate. The main following conclusions can be drawn:

– Except at RT, all hysteresis loops show serrations typical of Portevin le Chatelier bands occurrence during the plastic deformation which is not homogeneous.
– The evolution of the maximum stress with the number of cycles presents a first hardening followed by a stabilization and a second hardening. The first hardening is due to the cyclic strain hardening whereas the second hardening is attributed to DSA.
– The maximum stress amplitude is higher for the most sensitive steel in good agreement with the higher increase in Ultimate Tensile Stress measured on tensile tests.
– As in tensile tests, a negative strain rate sensitivity is seen in the LCF tests. When the strain rate decreases, the additional anchoring of the dislocations is higher.
– For our study and Lee and Kim [28], the DSA phenomenon enhances fatigue life (higher the sensitivity to DSA, higher the increase in fatigue life). Whereas, for some other authors and results, the DSA phenomenon reduces the fatigue life. Nevertheless, the decrease in strain rate always decreases the number of cycles to failure. This increase of fatigue life seems attributed to the hardness increase in the DSA domain (despite the ductility loss).

References

[1] Baird J. Strain ageing of steel – a critical review. Iron Steel 1963.
[2] Keh AS, Nakada Y, Leslie WC. Dynamic strain aging in iron and steel in dislocations dynamics. New York: Mc Graw-Hill; 1968. 381.
[3] Grumbach M, Sanz G. le vieillissement après écrouissage. C.I.T. du C.D.S. 1970;5:1285–341.
[4] Cuddy LJ, Leslie WC. Acta Metall Mater 1972;20:1157.
[5] Baird JD. The effects of strain ageing due to interstitial solutes on the mechanical properties of metals. Metall Rev 1971;149:1–18.
[6] Baird JD. Dynamic strain aging. In: ASM International, editor. The inhomogeneity of plastic deformation. Metals Park, Ohio; 1973. p. 191–222.
[7] Pickering FB. Low carbon mild steels in physical metallurgy and the design of steels. London: Applied Science Publishers Ltd; 1978. 52.
[8] Bocquet P, Gutmann M. Le vieillissement in Les aciers spéciaux. Ed lavoisier, Paris; 1997. p. 598–613.
[9] Wagner D, Moreno JC, Prioul C. Vieillissement dynamique dans les joints soudés d'aciers C–Mn. Influence de quelques paramètres métallurgiques sur le comportement en traction. Rev Metall 2000:1481–500.
[10] Wagner D, Moreno JC, Prioul C. Dynamic strain aging sensitivity of heat affected zones in C–Mn steels. J Nucl Mater 1998;252:257–65.
[11] Neuhäuser H, Schwink C. Solid solution strengthening. In: Cahn RW, Haasen P, Kramer EJ, editors. Materials science and technology, vol. 6; 1993.
[12] Brindley BJ, Worthington PJ. Metall Rev 1970;15:101–14.
[13] Cuddy LJ, Leslie WC. Acta Metall 1972;20:1157–67.
[14] Lacombe P. L'effet Portevin – Le Chatelier ses caractéristiques et ses conséquences sur les hétérogénéités de déformation plastique. In: Matériaux et Techniques; 1985. p. E5.
[15] Rodriguez P. Strain aging, dynamic. In: Cahn RW, editor. Encyclopedia of materials science and engineering-supplementary, vol. 1. Pergamon; 1988. p. 504–8.
[16] McCormick PG, Venkadesan S, Ling CP. Scr Metall Mater 1993;29:1159–64.
[17] Lebyodkin M, Dunin-Barkowskii L, Bréchet Y, Estrin Y, Kubin LP. Acta Mater 2000;48:2529–41.
[18] McCormick PG. Acta Metall 1972;20:351–4.
[19] Van den Beukel A. Phys Status Solidi 1975;30:197–206.
[20] Neuhäuser H. Plastic instabilities and the deformation of metals. In: Walgraef D, Ghoniem NM, editors. Patterns defects and material instabilities. Kluwer Academic Publishers; 1990. p. 241–76.
[21] Estrin Y, Kubin LP, Aifantis EC. Scr Metall Mater 1993;29:1147–50.
[22] Estrin Y, Kubin LP. Continuum models for materials and microstructure. In: Mühlhaus HB, editor. New York: Wiley; 1995. p. 395.
[23] Wagner D, Roubier N, Prioul C. Measurement of sensitivity to dynamic strain aging in C–Mn steels by internal friction experiments. Mater Sci Technol 2006;22(3):301–7.
[24] Leslie WC. Quench and strain aging in encyclopedia of materials science and engineering, vol. 5. Oxford: Pergamon Press; 1986. p. 4007–11.
[25] Marschall CW, Landow PP, Wilkowski GM. Effect of dynamic strain aging on fracture resistance of carbon steels operating at light-water reactor temperatures. ASTM STP 1990;1014:339–60.
[26] Abdel Raouf H, Plumtree A, Topper TH. Effect of temperature and deformation rate on cyclic strength and fracture of low carbon steel. Philadelphia, PA: ASTM STP 519; 1973. p. 28.
[27] Weisse M, Wamukwamba CK, Christ H-J, Mughrabi H. Acta Metall Mater 1993;41:2227.
[28] Lee BO, Kim IS. Dynamic strain aging in the high temperature low cycle fatigue of SA508 Cl.3 forging steel. J Nucl Mater 1995;226:216–25.
[29] Chopra OK, Shack WJ. Effect of LWR coolant environments on fatigue design curves of carbon and low alloy steels. Argonne National Laboratory, NUREG/CR-6583, ANL-97/18.
[30] Samuel KG, Ganesan V, Bhanu Sankara Rao K, Mannan SL, Kushwaha HS. Strain controlled LCF behaviour of SA-333Gr6 piping material in the range 298–673K. Int J Pressure Vessels Piping 2004;81:973–91.
[31] Chen L, Van der Pers NM, Bottger A, De Keijser ThH, Mittemeijer EJ. Lattice changes of iron–nitrogen martensite on ageing at room temperature. Metall Trans A 1990;21A:2857–67.
[32] Chen L, Van der Pers NM, Bottger A, De Keijser ThH, Mittemeijer EJ. Lattice changes of iron–carbon martensite on ageing at room temperature. Metall Trans A 1991;22A:1957–67.
[33] Chen L, Bottger A, Mittemeijer EJ. Tempering of iron–carbon–nitrogen martensites. Metall Trans A 1992;23A:1129–45.
[34] Fergusson P, Jack KH. Quench ageing and strain ageing of nitrogen ferrite. Proc Heat Treatment Conf., ed. The Metals Society, Birmingham; 1981. p. 158.
[35] Fast JD. Mét Cor Ind 1961;435:383.
[36] Mughrabi H. On the dislocation mechanisms of dynamic strain ageing in fatigued plain carbon steels. Z Metallkd 2003;94:5.
[37] Prioul C, Pasquet M, Carrard M, Plusquellec J, Azou P. Mem Et Sci Rev Metall 1982;79:203.
[38] Hertzberg RW, Vinci RP, JL. Deformation and fracture mechanics of engineering materials, 5th ed. John Wiley & Sons; 2012.